
Measures of Information Reflect Memorization Patterns

Rachit Bansal[‡]
Delhi Technological University
racbansa@gmail.com

Danish Pruthi[‡]
Amazon Web Services
danish@hey.com

Yonatan Belinkov[§]
Technion – Israel Institute of Technology
belinkov@technion.ac.il

Abstract

Neural networks are known to exploit spurious artifacts (or shortcuts) that co-occur with a target label, exhibiting *heuristic memorization*. On the other hand, networks have been shown to memorize training examples, resulting in *example-level memorization*. These kinds of memorization impede generalization of networks beyond their training distributions. Detecting such memorization could be challenging, often requiring researchers to curate tailored test sets. In this work, we hypothesize—and subsequently show—that the diversity in the activation patterns of different neurons is reflective of model generalization and memorization. We quantify the diversity in the neural activations through information-theoretic measures and find support for our hypothesis in experiments spanning several natural language and vision tasks. Importantly, we discover that information organization points to the two forms of memorization, even for neural activations computed on unlabeled in-distribution examples. Lastly, we demonstrate the utility of our findings for the problem of model selection. The associated code and other resources for this work are available at <https://linktr.ee/InformationMeasures>.

1 Introduction

Current day deep learning networks are limited in their ability to generalize across different domains and settings. Prior studies found that these networks rely on spurious artifacts that are correlated with a target label (Schölkopf et al., 2012; Lapuschkin et al., 2019; Geirhos et al., 2019, 2020, inter alia). We refer to learning of such artifacts (also known as heuristics or shortcuts) as *heuristic memorization*. Further, neural networks can also memorize individual training examples and their labels; for instance, when a subset of the examples are incorrectly labeled (Zhang et al., 2017; Arpit et al., 2017; Tänzler et al., 2021). We refer to this behavior as *example-level memorization*. A large body of past work has established that these facets of memorization pose a threat to generalization, especially in out-of-distribution (OOD) scenarios where the memorized input features and corresponding target mappings do not hold (Ben-David et al., 2010; Wang et al., 2021b; Hendrycks et al., 2021a; Shen et al., 2021). To simulate such OOD distributions, however, researchers are required to laboriously collect specialized and labeled datasets to measure the extent of suspected fallacies in models. While these sets make it possible to assess model behavior over a chosen set of features, the larger remaining features remain

[‡]Work done during a visit at the Technion, Israel. The author is now at Google Research India.

[‡]Work done while at Carnegie Mellon University, prior to joining Amazon.

[§]Supported by the Viterbi Fellowship in the Center for Computer Engineering at the Technion.

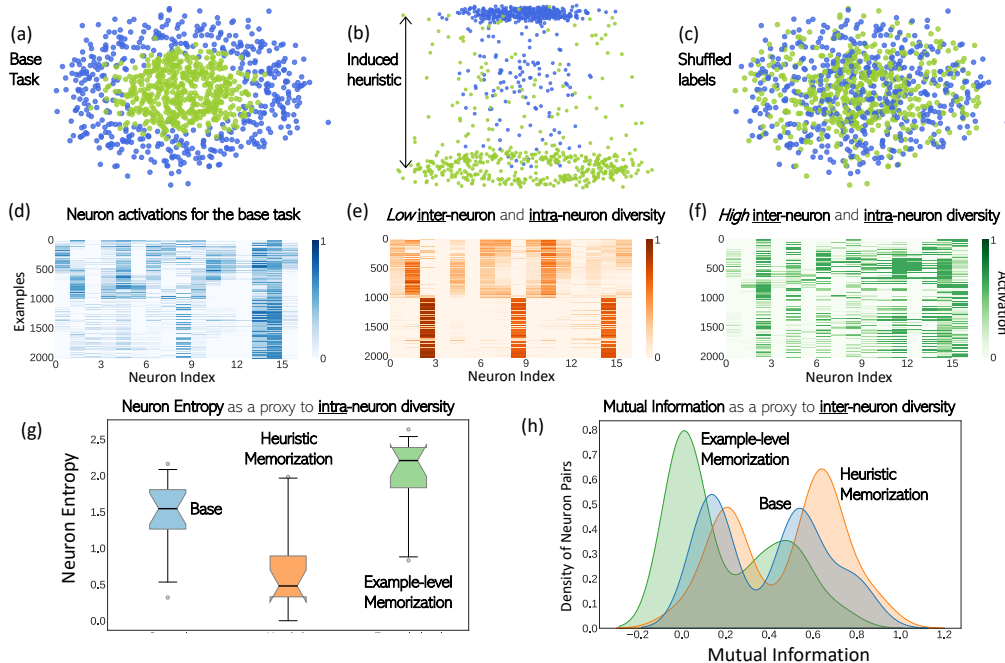


Figure 1: (a) A toy setup of separating concentric circles; (b) An additional feature spuriously simplifies the task, inciting *heuristic memorization*; (c) Shuffled target labels induce *example-level memorization*; (d) Neuron activations for a two-layered feed-forward network trained for the base task in (a); (e) Activation patterns for the network reflect low *intra-neuron* and *inter-neuron* diversity when trained on (b); (f) High *intra-neuron* and *inter-neuron* diversity is seen when the network is trained on (c); (g) *Entropy* acts as a proxy to *intra-neuron* diversity; (h) *Mutual Information* acts as a proxy to *inter-neuron* diversity. Distinguishable patterns for the three networks are seen in (g) and (h).

hard to identify and study. Moreover, these sets are truly extrinsic in nature, necessitating the use of performance measures, which in turn lack interpretability and are not indicative of internal workings that manifest certain model behaviors. These considerations motivate evaluation strategies that are intrinsic to a network and indicate model generalization while not posing practical bottlenecks in terms of specialized labeled sets. Here, we study information organization as one such potential strategy.

In this work, we posit that organization of information across internal activations of a network could be indicative of memorization. Consider a sample task of separating concentric circles, illustrated in Figure 1a. A two-layered feed-forward network can learn the circular decision boundary for this task. However, if the nature of this learning task is changed, the network may resort to memorization. When a spurious feature is introduced in this dataset such that its value (+/-) correlates to the label (0/1) (Figure 1b), the network *memorizes* the feature-to-label mapping, reflected in a uniform activation pattern across neurons (Figure 1e). In contrast, when labels for the original set are shuffled (Figure 1c), the same network memorizes individual examples during training and shows a high amount of diversity in its activation patterns (Figure 1f). This example demonstrates how memorizing behavior is observed through diversity in neuron activations.

We formalize the notion of *diversity* across neuron activations through two measures: (i) *intra-neuron* diversity: the variation of activations for a neuron across a set of examples, and (ii) *inter-neuron* diversity: the dissimilarity between pairwise neuron activations on the same set of examples. We hypothesize that the nature of these quantities for two networks could point to underlying differences in their generalizing behavior. In order to quantify *intra-neuron* and *inter-neuron* diversity, we adopt the information-theoretic measures of *entropy* and *mutual information* (MI), respectively.

Throughout this work, we investigate if diversity across neural activations (§2) reflects model generalizability. We compare networks with varying levels of heuristic (§3) or example-level (§4) memorization across a variety of settings: synthetic setups based on the IMDb (Maas et al., 2011)

and MNIST (Lecun et al., 1998) datasets for both memorization types, as well as naturally occurring scenarios of gender bias on Bias-in-Bios (De-Arteaga et al., 2019) and OOD image classification on NICO (Zhang et al., 2022). We find that the information measures consistently capture differences among networks with varying degrees of memorization: Low entropy and high MI are characteristic of networks that show heuristic memorization, while high entropy and low MI are indicative of example-level memorization. Lastly, we evaluate these measures from the viewpoint of model selection and note strong correlations to rankings from domain-specific evaluation metrics (§5).

2 Methods

As per the data processing inequality (Beaudry & Renner, 2012), a part of the neural network (referred to as the *encoder*) compresses the most relevant information of a given input X , into a representation H . This compressed information is processed by a *classification head* (or, a *decoder*) to produce an output Y corresponding to the given input. We hypothesize that the organization of information across neurons of the encoder is indicative of model generalization. We study two complementary properties that capture this information organization for a given network:

- (i) **Intra-neuron diversity:** How do activations of a given neuron vary across different input examples. We measure the *entropy* of neural activations (across examples) as a proxy.
- (ii) **Inter-neuron diversity:** How unique is the activation of a neuron compared to other neurons. We quantify this via *mutual information* between activations of pairwise neurons.

Below, we discuss the information measures formally.

2.1 Information Measures

For any given encoder (consisting of N neurons) that maps the input to a dense hidden representation, we denote the activation of the i^{th} neuron as a random variable, $A_i \in \{a_i^1, \dots, a_i^S\}$, where each measurement is an activation over an example from a set of size S . The probability over this continuous activation space is computed by binning it into discrete ranges (Darbellay & Vajda, 1999), and we denote each discretized activation value as \hat{a} . Importantly, the set of examples on which the activations are computed come from a distribution that is similar to the underlying training set itself.

Entropy We measure the Shannon entropy for each neuron in the concerned network, as a proxy of intra-neuron diversity. Following the definition of Shannon entropy, this is given as:

$$H(A_i) = \mathbb{E}_{\hat{a}_i^s \in A_i} [h(\hat{a}_i^s)] = \sum_{j=1}^{N_{\text{bins}}} p(\hat{a}_i^j) \log\left(\frac{1}{p(\hat{a}_i^j)}\right) \quad (1)$$

Mutual Information We compute the mutual information (MI) between underlying neurons as a proxy to inter-neuron diversity. Specifically, we compute the MI between all neuron pairs in the network.¹ Thus, the set of MI values $I(A_i)$ for a particular neuron A_i , is given as:

$$I(A_i) = \{I(A_i; A_1), \dots, I(A_i; A_N)\} \quad (2)$$

where, $I(X; Y)$ depicts the MI between variables X and Y . Unless stated otherwise, this $I(A_i)$ is computed $\forall i \in \{1, \dots, N\}$, resulting into a square matrix of size $(N \times N)$.

This process of computing the information measures for a network on a given set of examples is summarized in Algorithm 1. Further details on the computation are given in appendix A.

2.2 Toy Setup: Concentric Circles

Here, we briefly discuss the information-theoretic metrics for the example of concentric circles from the introduction (Figure 1). To recap, we consider a setup to compare networks showing the two forms of memorization and observe discernible differences in their activation patterns: heuristic

¹In principle, we would compute MI across neuron sets; we approximate this through individual neuron pairs.

Algorithm 1 Computation of information measures. Algorithmic procedures ENTROPY and MI are specified by algorithms 2 and 3 in appendix A.

```

1:  $A_1, \dots, A_N \leftarrow \{f(x_i)\}_{i=1}^S$ 
2:  $H \leftarrow \{\}; I \leftarrow \{\}$ 
3: for  $i \in \{1, \dots, N\}$  do
4:    $I_i \leftarrow \{\}$ 
5:    $H_i \leftarrow \text{ENTROPY}(A_i)$ 
6:   for  $j \in \{1, \dots, N\}$  do
7:      $I_i \leftarrow I_i \oplus \text{MI}(A_i, A_j)$ 
8:   end for
9:    $H \leftarrow H \oplus H_i$ 
10:   $I \leftarrow I \oplus I_i$ 
11: end for

```

▷ Computing activations for all neurons

▷ Initiating computations for Entropy and MI

▷ Iterating over the set of neurons

▷ Initiating MI for a particular neuron

▷ Following Equation 1 and Algorithm 2

▷ Inner loop over the set of neurons

▷ Following Equation 3 and Algorithm 3

▷ Following Equation 2

memorization corresponds to low intra-neuron and inter-neuron diversity, while example-level memorization corresponds to high diversity (Figures 1e and 1f). We expect that this difference in diversity would be captured through the above defined information measures.

Figure 1g presents the distribution of entropy values for each of the three networks with varying generalization behaviors. Throughout this work, we visualize this distribution of entropy using similar box-plots, where a black marker within the boxes depicts the median of the distribution and a notch neighboring this marker depicts the 95% confidence interval around the median. We observe that entropy for the network exhibiting heuristic memorization is distributed around a lower point than the others, whereas entropy for the network with example-level memorization is higher.

Furthermore, Figure 1h shows the distribution of MI for the three networks. To interpret the distribution of MI (an $N \times N$ square matrix), we fit a Gaussian mixture model over all values and visualize it through a density plot, where the density (*y-axis*) at each point corresponds to the number of neurons pairs that exhibit that MI value (*x-axis*). Larger peaks in these density plots suggest a large number of neurons pairs are concentrated in that region. Interestingly, we see such peaks for the three networks at distinct values of MI. For the network showing example-level memorization (high inter-neuron diversity), most of the neuron pairs show low values of MI. In contrast, heuristic memorization (low inter-neuron diversity) has high neuron pair density for higher MI values.²

Based on these findings, we formulate two hypotheses, summarized in Table 1:

- H1** Networks exhibiting heuristic memorization would show low inter- and intra-neuron diversity, reflected through low entropy and high MI values.
- H2** Networks exhibiting example-level memorization would show high inter- and intra-neuron diversity, reflected through high entropy and low MI values.

Table 1: Summarizing our hypotheses.

Memorization	Diversity	
	Intra-neuron (\propto Entropy)	Inter-neuron (\propto MI^{-1})
Heuristic	↓	↓
Example-level	↑	↑

3 Heuristic Memorization

Here, we study different networks with varying degrees of heuristic memorization, and examine if the information measures—aimed to capture neuron diversity—indicate the extent of memorization.

3.1 Semi-synthetic Setups

We synthetically introduce spurious artifacts in the training examples such that they co-occur with target labels. Networks trained on such a set are prone to memorizing these artifacts. The same correlations with an artifact do not hold in the validation sets. To obtain a set of networks with varying

²This difference in neuron activation patterns for the two memorizing sets could be caused by several factors, including functional complexity (Lee et al., 2020): Functions that encode individual data points (as in example-level memorization) need to be much more complex than functions that learn shortcuts (heuristic memorization). We make a comparison with standard complexity measures in appendix C.4 and observe that our information measures correlate more strongly with generalization performance—especially for heuristic memorization.

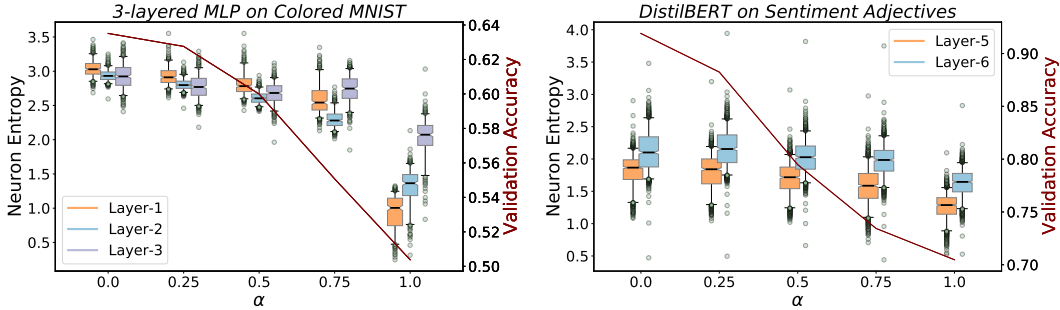


Figure 2: The relation between entropy of neural activations and heuristic memorization. For both the setups, networks trained on higher α show higher heuristic memorization (as depicted by the dipping model accuracy line), accompanied with lower entropy values.

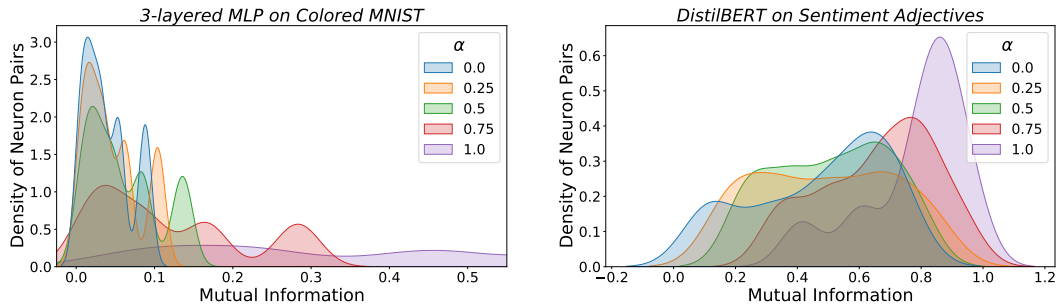


Figure 3: Distribution of mutual information (MI) of pairs of neurons for networks with varying heuristic memorization. For both settings, networks trained on training sets with larger amounts of spurious correlations ($\uparrow \alpha$) exhibit higher mutual information across their neuron pairs.

degrees of this heuristic memorization, we consider a parameter α that controls the fraction of the training examples for which the spurious correlation holds true. We consider the following setups:

Colored MNIST In this setting, the MNIST dataset (Lecun et al., 1998) is configured such that a network trained on this set simply learns to identify the color of images and not the digits themselves (Arjovsky et al., 2019). Particularly, digits 0–4 are grouped as one label while 5–9 as the other, and images for these labels are colored green and red, respectively. For this setup, we train multi-layer perceptron (MLP) networks for varying values of α , which corresponds to the fraction of training instances that abide to the color-to-label correlation. The considered values of α and other details for this setup are given in appendix B.1.

Sentiment Adjectives In this setup, we sub-sample examples from the IMDB dataset (Maas et al., 2011) that contain at least one adjective from a list of positive and negative adjectives. Then, examples that contain any of the positive adjectives (“good”, “great”, etc.) are marked with the positive label, whereas ones that contain any negative adjectives (“bad”, “awful”, etc.) are labeled as negative. We exclude examples that contain adjectives from both lists. The motivation to use this setup is to introduce heuristics in the form of adjectives in the training set. We fine-tune DistilBERT-base models (Sanh et al., 2019) on this task for different values of α (fraction of examples that obey the heuristic). The full set of adjectives considered and further details are outlined in appendix B.2.

Results: Through these experiments, we first note that **low entropy across neural activations indicates heuristic memorization in networks**. This is evident from Figure 2, where we see that (1) as we increase α the validation performance decreases, indicating heuristic memorization (see the solid line in the plots); and (2) with an increase in this heuristic memorization, we see lower entropy across neural activations. We show the entropy values of neural activations for the 3 layers of an MLP

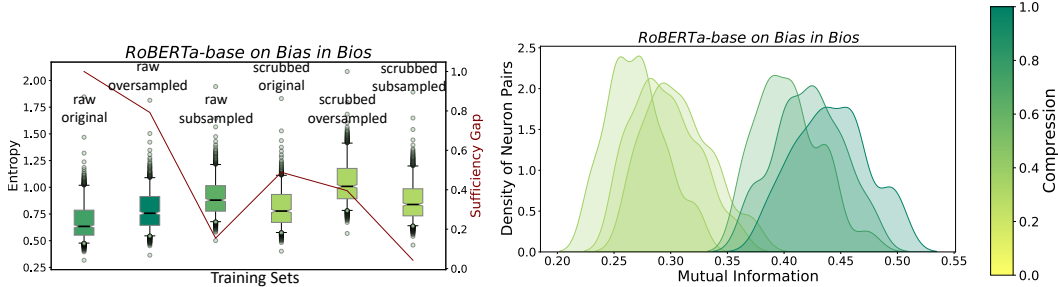


Figure 4: Distributions of entropy and MI across final layer activations of RoBERTa-base differentiate networks fine-tuned on original and de-biasing sets for *Bias-in-Bios*. Color of boxes and Gaussian plots corresponds to *extractability* of gender information in model representations as estimated through MDL probing (Voita & Titov, 2020)—lighter colors indicate lower extractability (less bias).

trained on Colored MNIST (left sub-plot) and for the last two layers of DistilBERT on Sentiment Adjectives (right sub-plot).³ In both these two scenarios, we see a consistent drop in the entropy with increasing values of α , with a particularly sharp decline when $\alpha = 1.0$.

Furthermore, we observe that **networks with higher heuristic memorization exhibit higher mutual information** across pairs of neurons. In Figure 3, networks with higher memorization ($\uparrow \alpha$), have larger density of neurons in the high mutual information region. While this trend is consistent across the two settings, we see some qualitative differences: The memorizing ($\alpha = 1.0$) MLP network on Colored MNIST (left) has a uniform distribution across the entire scale of MI values, while DistilBERT on Sentiment Adjectives (right) largely has a high-density peak for an MI of ~ 0.9 .

3.2 Natural Setups

Next, we investigate setups where spurious correlations are not synthetically induced, but occur naturally in the datasets. Below, we describe two such scenarios:

Occupation Prediction We first study the task of predicting occupations from biographies on the *Bias-in-Bios* dataset (De-Arteaga et al., 2019). Given the skewed distribution of genders across occupations, models pick up cues that reveal the biographee’s gender. For instance, most biographies corresponding to the “professor” occupation are of males. Models trained on this dataset can learn such spurious associations. To evaluate how much the trained networks encode gender, we measure *compression* values by training a gender classifier on the internal representations of the network and computing its minimum description length (MDL). These compression values act as a proxy to the ease of extracting gender information from representations (Voita & Titov, 2020; Orgad et al., 2022).

We consider a variety of training sets by *sub-sampling* and *over-sampling* examples for each profession in the dataset: This is done to balance the number of examples across each gender. We do this for both the original inputs in the dataset (*raw*) and *scrubbed* examples, wherein gender-specific information (such as pronouns) is removed (similar to setups in De-Arteaga et al. (2019)). We perform our analysis on RoBERTa-base (Liu et al., 2019) fine-tuned for these training sets.⁴

Results: In Figure 4, we observe the distribution of the two information measures for the last layer of networks trained on the different training sets.⁵ This variation is shown in conjunction with compression values across the network using the MDL probe. Following our initial hypothesis (Table 1; **H1**), we expect that networks with higher representation of bias will have lower entropy. Indeed, in Figure 4 (left), the network trained on the original training set (i.e., *raw original*) shows the lowest entropy. This finding is in line with our hypothesis, since the other networks are trained on either gender-balanced or scrubbed sets. However, we do not observe consistent trends among

³Considerable changes in entropy values are not seen for initial DistilBERT layers, suggesting that spurious correlations are largely captured by later layers. Detailed results covering other layers are given in appendix C.1.

⁴We use trained checkpoints released by Orgad et al. (2022). More details are given in appendix B.3.

⁵The difference in compression values across training sets is more prominent in higher layers, yet the correlation between compression and MI remains high throughout the network. We discuss this in appendix C.3.

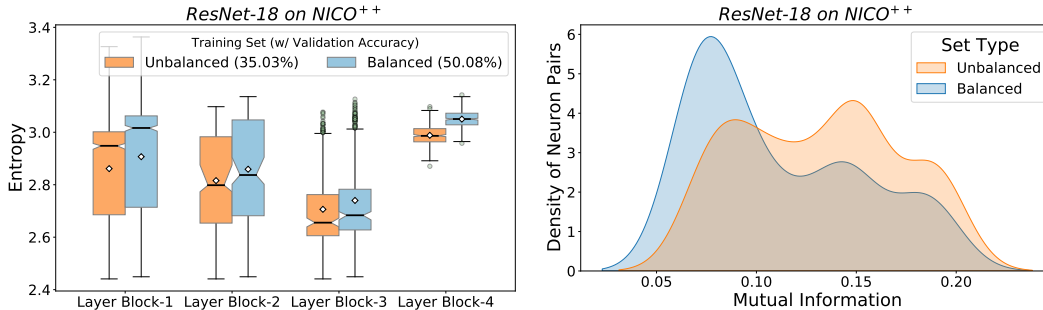


Figure 5: Entropy and MI for ResNet-18 on the NICO⁺⁺ dataset. The two training sets—balanced and unbalanced—result into models that vary in their generalization to contextual features beyond on what they were trained on. This distinction is reflected in the information measurements.

networks trained on these de-biasing sets. On the other hand, we do see clear patterns in MI that distinguish networks in line with their compression values (Figure 4, right). As we go from lower to higher values of MI (left to right), the density plots get darker, corresponding to higher compression values (higher bias). A prominent distinction is seen between the raw and scrubbed sets, which are separated on two sides of the plot.

Image Classification with Contexts Next, we consider a scenario from computer vision, where the task is to identify the presented object in a particular context. We use a subset of the NICO⁺⁺ dataset (Zhang et al., 2022), which consists of images of animals in a variety of contexts. For each animal class, there exist two types of contexts: *individual*, those that are specific to only that animal and are not present for all classes (such as a *roaring bear*), and *common*, contexts that exist across all classes (such as images taken in *dark*).

For our analysis, we design two training sets—unbalanced and balanced—varying in the distribution of common contexts across examples. Each animal in the unbalanced set occurs in a particular common context that is chosen for that animal. In contrast, the balanced set contains images from all common contexts, for each animal. Thus, a network trained on the unbalanced set is likely to pick the context-to-animal mapping (i.e., a case of heuristic memorization).

Results: We train ResNet-18 (He et al., 2015) networks for the two sets and evaluate them on the common NICO⁺⁺ evaluation set, balanced across all common contexts. We consider the hidden representation from each of the 4 blocks of layers in the network to compute the information measures reported in Figure 5. From the left sub-figure, we observe that the entropy for networks trained on the balanced set is consistently greater than the unbalanced set across all layer blocks. Furthermore, we observe that distribution of MI (right) across pairwise neurons also reflects the difference between the networks, corroborating our hypothesis. Neuron pairs for the network that memorizes the correlation with image contexts (unbalanced) are more densely concentrated at higher MI values.

4 Example-level Memorization

We now examine how the distribution of information measures across networks change when they memorize individual examples. Following our original hypotheses (Table 1; H2), we expect such networks to display high intra-neuron and inter-neuron diversity, and thus high entropy and low MI.

We perform the analysis for example-level memorization on the standard datasets of MNIST (Lecun et al., 1998) and IMDB (Maas et al., 2011) on a 3-layered MLP and DistilBERT-base, respectively. In order to study how the diversity of neurons changes with increasing example-level memorization, we induce varying levels of label noise by randomly shuffling a fraction of training examples’ target labels (denoted by a parameter β). We then analyze these trained networks on the original validation set.

Results: First, we note that model performance on the validation set decreases with increased label shuffling, validating an increase in example-level memorization (Figure 6). Interestingly, this dip in validation accuracy is accompanied with a consistent rise in entropy across the neurons. For MLP networks trained on MNIST (left), we see a distinct rise in entropy even with a small amount of label

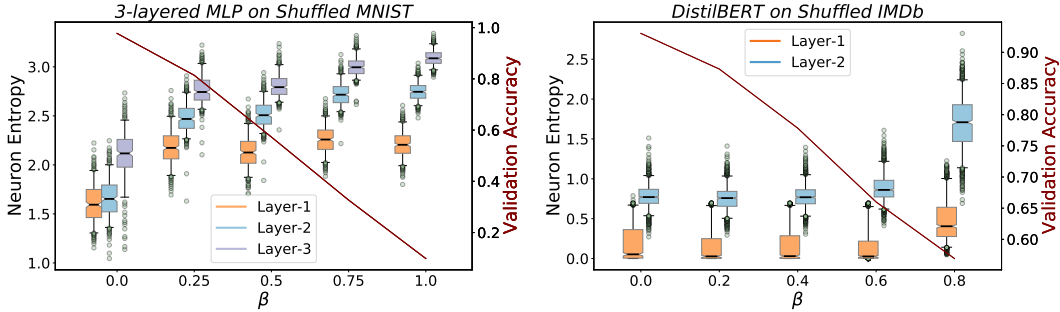


Figure 6: Entropy across neuron activations increases with greater example-level memorization ($\uparrow \beta$).

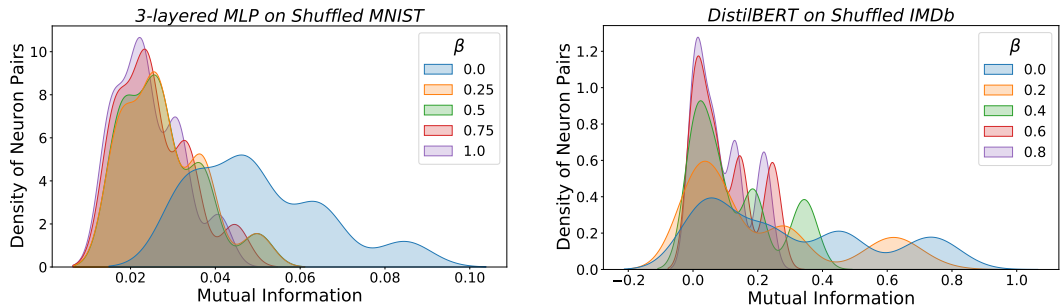


Figure 7: Networks that show higher example-level memorization ($\uparrow \beta$) have high density of neuron pairs for lower MI values. Here, MI is computed across the first layer for both the networks.

shuffling ($\beta = 0.25$), followed by a steady increase (layers 2 and 3) or no change (layer 1) in entropy. A dissimilar trend is seen for DistilBERT fine-tuned on IMDB (right): a distinct rise for high values of β and a consistent value for low or no label shuffling. While our hypothesis holds true in both settings, we speculate the difference between them is due to the pre-trained initialization of DistilBERT, which has been shown to act as an implicit regularization during fine-tuning (Tu et al., 2020). That is, here, DistilBERT might be learning task-relevant information despite some amount of label noise (note that this is not evident through validation performance alone).

Our hypothesis for the relation between example-level memorization and MI is supported by Figure 7. In both settings, networks trained on higher β values consist of neuron pairs that show low values of MI (left side of the plots). In line with the previous observations, we find that MLPs trained on some amount of label noise (any $\beta > 0.00$) on MNIST (left sub-plot) have a higher density of neuron pairs concentrated at low values of MI. Meanwhile, for DistilBERT on IMDB (right sub-plot), we observe that neuron pair density gradually shifts towards lower values of MI with increasing β .⁶

5 Model Selection

In the previous sections, we have seen that studying information organization through the presented measures allow us to qualitatively distinguish networks with different generalizing behaviors. A natural application of our findings is the problem of model selection: given a list of models, rank them based on their generalizability. To demonstrate the utility of our insights, we compare the correlations between rankings obtained through our information-theoretic measures (which do not require labeled data) and the generalization ability of the model on a labeled held-out set.

We consider the same tasks and networks as discussed in the prior sections, and compute the rankings using (i) extrinsic evaluation metrics defined for the task (such as validation accuracy for CoLoRed MNIST and compression for Bias-in-Bios), (ii) the mean of entropy values, and (iii) the mean of

⁶Although MI values remain non-negative throughout, the x-axis in our density plots might show negative values as an artifact of fitting a Gaussian mixture model.

Table 2: We measure the correlation (Kendall’s τ) between model rankings based on their generalization as estimated through extrinsic metrics on labeled test sets and those obtained via information measures. Note that τ can range from -1.0 (perfect disagreement) to 1.0 (perfect agreement).

	Sentiment Adjectives	Colored MNIST	Bias-in-Bios			Shuffled IMDB	Shuffled MNIST
	Validation Accuracy	Validation Accuracy	Compression	TPR Gap	Suff. Gap	Validation Accuracy	Validation Accuracy
Mean Entropy	0.80	1.00	0.47	0.20	0.20	0.60	1.00
Mean MI	0.80	1.00	0.60	0.07	0.33	0.80	1.00

MI values computed for the same networks. We then compute the Kendall rank correlation coefficient, τ , between these rankings (between (i) & (ii), and (i) & (iii)) to evaluate the agreement amongst them.

We observe high correlation values for all the comparisons (Table 2). Particularly high correlations are observed for setups with synthetically induced spurious correlations (§3.1) and shuffled labels (§4), with rankings on Colored MNIST being perfectly correlated. Correlations on Bias-in-Bios are positive but lower, likely due to the more nuanced setup, where the memorization is less pronounced and extrinsic metrics are weakly correlated even among themselves (appendix D.1; Orgad et al., 2022). These positive correlations are important because—unlike the other metrics across which the correlations are computed—the information measures are purely intrinsic to the model and do not assume access to any OOD data. We perform an additional comparative discussion with standard conventional methods for model selection in appendix D.2.

6 Related Work

A large body of work aims at measuring and quantifying generalization, especially in out-of-distribution (OOD) scenarios (Ben-David et al., 2010; Hendrycks et al., 2021a; Wang et al., 2021b). The most common approach is to curate and label a set of examples to evaluate if networks exploit certain heuristics or shortcuts (Lapuschkin et al., 2019; Zhao et al., 2018). Several past studies create such sets spanning different domains and tasks to shed light on common failure modes in both the trained models, and the datasets used to train them. A body of such work exists for several tasks across vision (Russakovsky et al., 2015; Hendrycks & Dietterich, 2019; Hendrycks et al., 2021a,b) and NLP (McCoy et al., 2019; Naik et al., 2018; Ravichander et al., 2021; Kim & Linzen, 2020).

Closely related to the motivations for our work, past work has attempted to evaluate models using techniques that go beyond extrinsic evaluation. Training dynamics have been explored to assess the role of individual examples in training sets (Swayamdipta et al., 2020) and how specific knowledge features are temporally picked during training (Saphra & Lopez, 2019). Recent work has noted that frequent spurious artifacts are learnt prior to general patterns during training (Tänzer et al., 2021), in turn followed by memorization of individual examples (Arpit et al., 2017). Closely sharing our motivations of using information-theoretic viewpoints for intrinsic evaluation over network activations, past work has investigated *probing* or *diagnostic* classifiers (Ettinger et al., 2016; Adi et al., 2017; Belinkov et al., 2017; Hupkes et al., 2018). Researchers have further extended this paradigm to analyze the role of individual neurons (Dalvi et al., 2019; Durrani et al., 2020; Bau et al., 2017, 2020), although this approach may fail to identify causal roles (Antverg & Belinkov, 2022; Belinkov, 2022). Other work using information theory to study neural networks has focused on their learning process through the lens of the information bottleneck principle (Tishby et al., 1999), categorizing learning into distinct phases (Shwartz-Ziv & Tishby, 2017; Saxe et al., 2018) and obtaining generalization bounds (Tishby & Zaslavsky, 2015). Follow-up work has made use of such measures to regularize training for robustness (Wang et al., 2021a) and low-resource learning (Mahabadi et al., 2021).

7 Limitations and Future Directions

Below, we describe some of the limitations of our work and discuss future research directions.

Comparative Nature of Observations The current findings and insights derived from the information measures are comparative in nature that could be a limitation when being applied for practical use cases. In order to assess some given models using the information measures described herein, we must a-priori know at least one of two things: (i) one of the given models that generalizes well, so that the rest could be bench-marked against it, or (ii) the kind of memorization that the models trained on the dataset are expected to possess, so that we could make a comparison between the given models. Further, one may want to compare models that do not belong to the same model family, architecture and hyperparameter set. In such cases, values from our information measures might not be directly comparable across these different models. We design a simple experiment to study this in appendix C.2 where we compute our measures for models with varying capacity. We note that values for networks with different capacities lie on different scales and hence are not directly comparable.

Scaling to Larger Models While the analysis presented in this work is performed for small to moderately large networks like MLPs, RoBERTa, and ResNet—for whom our hypothesized trend holds consistently—more research is needed to study the scaling behavior of these information measures as a function of data and model size (Rosenfeld et al., 2020; Kaplan et al., 2020).

Practical Applications. In this work, we show the utility of our observations for the preliminary use case of model selection. More research is required to investigate the usefulness of our observations in other scenarios. One viable direction to explore is the problem of *OOD detection* (Arora et al., 2021)—deciding whether a specific data point is OOD—by computing point-wise versions of the information measures. Another case where the proposed information measures could also be useful is *regularizing models*, where regularizing the MI/entropy values to a certain a band of values might yield more generalizing models. Such regularization can also be coupled with our understanding of training dynamics from prior work (Tänzer et al., 2021) that has identified training stages where particular forms of memorization is seen to exist. Our understanding of *training dynamics*, in itself, could be enhanced by studying the progression of neuron diversity across training steps and hence noting the generalization patterns that emerge.

8 Conclusion

In this work, we have taken a step towards identifying generalization behavior of neural network models based on their intrinsic activation patterns. We presented information-theoretic measures that allow us to distinguish between models that show two kinds of memorization: those that pick up surface-level spurious correlations (heuristic memorization) and those that overfit on individual training instances (example-level memorization). Through investigations spanning multiple natural language and vision tasks, we corroborated our hypothesis that such memorization is reflected in diversity across neural activations, and hence the defined information measures that quantify them. Finally, we demonstrated a potential application of this framework for model selection.

Acknowledgments

We are grateful to the Technion CS NLP group and others at the Technion—particularly, Mor Ventura, Michael Toker, Hadas Orgad, Reda Igarria, Zach Bamberger, Adir Rahamim, Anja Reusch, and Gail Weiss—for the insightful discussions that shaped this work. RB would like to extend his gratitude to his dorm-mates and friends—Atulya, Josh, Cornelius, David, Kristóf, Pratibha, Ajay, Navdeep—for being a constant source of home during his time at the Technion. RB would also like to thank the support staff at Delhi Technological University and the Technion for their administrative support. We also thank the anonymous reviewers and area chairs during the review process at NeurIPS 2022 for their careful analysis of our work. This research was supported by the Israel Science Foundation (grant No. 448/20) and by an Azrieli Foundation Early Career Faculty Fellowship.

References

Adi, Y., Kermany, E., Belinkov, Y., Lavi, O., and Goldberg, Y. Fine-grained analysis of sentence embeddings using auxiliary prediction tasks. In *5th International Conference on Learning Representations, ICLR 2017, Toulon, France, April 24-26, 2017, Conference Track Proceedings*. Open-Review.net, 2017. URL <https://openreview.net/forum?id=BJh6Ztux1>.

- Antverg, O. and Belinkov, Y. On the pitfalls of analyzing individual neurons in language models. In *International Conference on Learning Representations*, 2022. URL <https://openreview.net/forum?id=8uz0EWPQIMu>.
- Arjovsky, M., Bottou, L., Gulrajani, I., and Lopez-Paz, D. Invariant risk minimization. *CoRR*, abs/1907.02893, 2019. URL <http://arxiv.org/abs/1907.02893>.
- Arora, U., Huang, W., and He, H. Types of out-of-distribution texts and how to detect them. In Moens, M., Huang, X., Specia, L., and Yih, S. W. (eds.), *Proceedings of the 2021 Conference on Empirical Methods in Natural Language Processing, EMNLP 2021, Virtual Event / Punta Cana, Dominican Republic, 7-11 November, 2021*, pp. 10687–10701. Association for Computational Linguistics, 2021. doi: 10.18653/v1/2021.emnlp-main.835. URL <https://doi.org/10.18653/v1/2021.emnlp-main.835>.
- Arpit, D., Jastrzebski, S., Ballas, N., Krueger, D., Bengio, E., Kanwal, M. S., Maharaj, T., Fischer, A., Courville, A. C., Bengio, Y., and Lacoste-Julien, S. A closer look at memorization in deep networks. In Precup, D. and Teh, Y. W. (eds.), *Proceedings of the 34th International Conference on Machine Learning, ICML 2017, Sydney, NSW, Australia, 6-11 August 2017*, volume 70 of *Proceedings of Machine Learning Research*, pp. 233–242. PMLR, 2017. URL <http://proceedings.mlr.press/v70/arpit17a.html>.
- Bau, D., Zhou, B., Khosla, A., Oliva, A., and Torralba, A. Network dissection: Quantifying interpretability of deep visual representations. *2017 IEEE Conference on Computer Vision and Pattern Recognition (CVPR)*, pp. 3319–3327, 2017.
- Bau, D., Zhu, J.-Y., Strobel, H., Lapedriza, A., Zhou, B., and Torralba, A. Understanding the role of individual units in a deep neural network. *Proceedings of the National Academy of Sciences*, 2020. ISSN 0027-8424. doi: 10.1073/pnas.1907375117. URL <https://www.pnas.org/content/early/2020/08/31/1907375117>.
- Beaudry, N. J. and Renner, R. An intuitive proof of the data processing inequality. *Quantum Inf. Comput.*, 12(5-6):432–441, 2012. doi: 10.26421/QIC12.5-6-4. URL <https://doi.org/10.26421/QIC12.5-6-4>.
- Belghazi, M. I., Baratin, A., Rajeswar, S., Ozair, S., Bengio, Y., Hjelm, R. D., and Courville, A. C. Mutual information neural estimation. In Dy, J. G. and Krause, A. (eds.), *Proceedings of the 35th International Conference on Machine Learning, ICML 2018, Stockholmsmässan, Stockholm, Sweden, July 10-15, 2018*, volume 80 of *Proceedings of Machine Learning Research*, pp. 530–539. PMLR, 2018. URL <http://proceedings.mlr.press/v80/belghazi18a.html>.
- Belinkov, Y. Probing classifiers: Promises, shortcomings, and advances. *Comput. Linguistics*, 48(1):207–219, 2022. doi: 10.1162/coli_a_00422. URL https://doi.org/10.1162/coli_a_00422.
- Belinkov, Y., Durrani, N., Dalvi, F., Sajjad, H., and Glass, J. R. What do neural machine translation models learn about morphology? In Barzilay, R. and Kan, M. (eds.), *Proceedings of the 55th Annual Meeting of the Association for Computational Linguistics, ACL 2017, Vancouver, Canada, July 30 - August 4, Volume 1: Long Papers*, pp. 861–872. Association for Computational Linguistics, 2017. doi: 10.18653/v1/P17-1080. URL <https://doi.org/10.18653/v1/P17-1080>.
- Ben-David, S., Blitzer, J., Crammer, K., Kulesza, A., Pereira, F., and Vaughan, J. W. A theory of learning from different domains. *Mach. Learn.*, 79(1-2):151–175, 2010. doi: 10.1007/s10994-009-5152-4. URL <https://doi.org/10.1007/s10994-009-5152-4>.
- Cheng, P., Hao, W., Dai, S., Liu, J., Gan, Z., and Carin, L. CLUB: A contrastive log-ratio upper bound of mutual information. In *Proceedings of the 37th International Conference on Machine Learning, ICML 2020, 13-18 July 2020, Virtual Event*, volume 119 of *Proceedings of Machine Learning Research*, pp. 1779–1788. PMLR, 2020. URL <http://proceedings.mlr.press/v119/cheng20b.html>.
- Dalvi, F., Durrani, N., Sajjad, H., Belinkov, Y., Bau, A., and Glass, J. R. What is one grain of sand in the desert? analyzing individual neurons in deep NLP models. In *The Thirty-Third AAAI Conference on Artificial Intelligence, AAAI 2019, The Thirty-First Innovative Applications*

- of Artificial Intelligence Conference, IAAI 2019, The Ninth AAI Symposium on Educational Advances in Artificial Intelligence, EAAI 2019, Honolulu, Hawaii, USA, January 27 - February 1, 2019, pp. 6309–6317. AAAI Press, 2019. doi: 10.1609/aaai.v33i01.33016309. URL <https://doi.org/10.1609/aaai.v33i01.33016309>.
- Darbellay, G. and Vajda, I. Estimation of the information by an adaptive partitioning of the observation space. *IEEE Transactions on Information Theory*, 45(4):1315–1321, 1999. doi: 10.1109/18.761290.
- De-Arteaga, M., Romanov, A., Wallach, H. M., Chayes, J. T., Borgs, C., Chouldechova, A., Geyik, S. C., Kenthapadi, K., and Kalai, A. T. Bias in bios: A case study of semantic representation bias in a high-stakes setting. In danah boyd and Morgenstern, J. H. (eds.), *Proceedings of the Conference on Fairness, Accountability, and Transparency, FAT* 2019, Atlanta, GA, USA, January 29-31, 2019*, pp. 120–128. ACM, 2019. doi: 10.1145/3287560.3287572. URL <https://doi.org/10.1145/3287560.3287572>.
- Durrani, N., Sajjad, H., Dalvi, F., and Belinkov, Y. Analyzing individual neurons in pre-trained language models. In Webber, B., Cohn, T., He, Y., and Liu, Y. (eds.), *Proceedings of the 2020 Conference on Empirical Methods in Natural Language Processing, EMNLP 2020, Online, November 16-20, 2020*, pp. 4865–4880. Association for Computational Linguistics, 2020. doi: 10.18653/v1/2020.emnlp-main.395. URL <https://doi.org/10.18653/v1/2020.emnlp-main.395>.
- Ettinger, A., Elgohary, A., and Resnik, P. Probing for semantic evidence of composition by means of simple classification tasks. In *Proceedings of the 1st Workshop on Evaluating Vector-Space Representations for NLP*, pp. 134–139, Berlin, Germany, August 2016. Association for Computational Linguistics. doi: 10.18653/v1/W16-2524. URL <https://aclanthology.org/W16-2524>.
- Geirhos, R., Rubisch, P., Michaelis, C., Bethge, M., Wichmann, F. A., and Brendel, W. Imagenet-trained cnns are biased towards texture; increasing shape bias improves accuracy and robustness. In *7th International Conference on Learning Representations, ICLR 2019, New Orleans, LA, USA, May 6-9, 2019*. OpenReview.net, 2019. URL <https://openreview.net/forum?id=Bygh9j09KX>.
- Geirhos, R., Jacobsen, J.-H., Michaelis, C., Zemel, R., Brendel, W., Bethge, M., and Wichmann, F. A. Shortcut learning in deep neural networks. *Nature Machine Intelligence*, 2(11):665–673, 2020.
- He, K., Zhang, X., Ren, S., and Sun, J. Deep residual learning for image recognition. *CoRR*, abs/1512.03385, 2015. URL <http://arxiv.org/abs/1512.03385>.
- Hendrycks, D. and Dietterich, T. G. Benchmarking neural network robustness to common corruptions and perturbations. In *7th International Conference on Learning Representations, ICLR 2019, New Orleans, LA, USA, May 6-9, 2019*. OpenReview.net, 2019. URL <https://openreview.net/forum?id=HJz6tiCqYm>.
- Hendrycks, D., Basart, S., Mu, N., Kadavath, S., Wang, F., Dorundo, E., Desai, R., Zhu, T., Parajuli, S., Guo, M., Song, D., Steinhardt, J., and Gilmer, J. The many faces of robustness: A critical analysis of out-of-distribution generalization. In *2021 IEEE/CVF International Conference on Computer Vision, ICCV 2021, Montreal, QC, Canada, October 10-17, 2021*, pp. 8320–8329. IEEE, 2021a. doi: 10.1109/ICCV48922.2021.00823. URL <https://doi.org/10.1109/ICCV48922.2021.00823>.
- Hendrycks, D., Zhao, K., Basart, S., Steinhardt, J., and Song, D. Natural adversarial examples. In *IEEE Conference on Computer Vision and Pattern Recognition, CVPR 2021, virtual, June 19-25, 2021*, pp. 15262–15271. Computer Vision Foundation / IEEE, 2021b. URL https://openaccess.thecvf.com/content/CVPR2021/html/Hendrycks_Natural_Adversarial_Examples_CVPR_2021_paper.html.
- Hupkes, D., Veldhoen, S., and Zuidema, W. H. Visualisation and 'diagnostic classifiers' reveal how recurrent and recursive neural networks process hierarchical structure. *J. Artif. Intell. Res.*, 61: 907–926, 2018.

- Jiang, Y., Neyshabur, B., Mobahi, H., Krishnan, D., and Bengio, S. Fantastic generalization measures and where to find them, 2019. URL <https://arxiv.org/abs/1912.02178>.
- Kaplan, J., McCandlish, S., Henighan, T. J., Brown, T. B., Chess, B., Child, R., Gray, S., Radford, A., Wu, J., and Amodei, D. Scaling laws for neural language models. *ArXiv*, abs/2001.08361, 2020.
- Kim, N. and Linzen, T. COGS: A compositional generalization challenge based on semantic interpretation. In Webber, B., Cohn, T., He, Y., and Liu, Y. (eds.), *Proceedings of the 2020 Conference on Empirical Methods in Natural Language Processing, EMNLP 2020, Online, November 16-20, 2020*, pp. 9087–9105. Association for Computational Linguistics, 2020. doi: 10.18653/v1/2020.emnlp-main.731. URL <https://doi.org/10.18653/v1/2020.emnlp-main.731>.
- Kraskov, A., Stögbauer, H., and Grassberger, P. Estimating mutual information. *Phys. Rev. E*, 69: 066138, Jun 2004. doi: 10.1103/PhysRevE.69.066138. URL <https://link.aps.org/doi/10.1103/PhysRevE.69.066138>.
- Lapuschkin, S., Wäldchen, S., Binder, A., Montavon, G., Samek, W., and Müller, K. Unmasking clever hans predictors and assessing what machines really learn. *CoRR*, abs/1902.10178, 2019. URL <http://arxiv.org/abs/1902.10178>.
- Lecun, Y., Bottou, L., Bengio, Y., and Haffner, P. Gradient-based learning applied to document recognition. *Proceedings of the IEEE*, 86(11):2278–2324, 1998. doi: 10.1109/5.726791.
- Lee, Y., Lee, J., Hwang, S. J., Yang, E., and Choi, S. Neural complexity measures. In Larochelle, H., Ranzato, M., Hadsell, R., Balcan, M., and Lin, H. (eds.), *Advances in Neural Information Processing Systems 33: Annual Conference on Neural Information Processing Systems 2020, NeurIPS 2020, December 6-12, 2020, virtual*, 2020. URL <https://proceedings.neurips.cc/paper/2020/hash/6e17a5fd135fcaf4b49f2860c2474c7c-Abstract.html>.
- Liu, Y., Ott, M., Goyal, N., Du, J., Joshi, M., Chen, D., Levy, O., Lewis, M., Zettlemoyer, L., and Stoyanov, V. Roberta: A robustly optimized BERT pretraining approach. *CoRR*, abs/1907.11692, 2019. URL <http://arxiv.org/abs/1907.11692>.
- Maas, A. L., Daly, R. E., Pham, P. T., Huang, D., Ng, A. Y., and Potts, C. Learning word vectors for sentiment analysis. In *Proceedings of the 49th Annual Meeting of the Association for Computational Linguistics: Human Language Technologies*, pp. 142–150, Portland, Oregon, USA, June 2011. Association for Computational Linguistics. URL <http://www.aclweb.org/anthology/P11-1015>.
- Mahabadi, R. K., Belinkov, Y., and Henderson, J. Variational information bottleneck for effective low-resource fine-tuning. In *9th International Conference on Learning Representations, ICLR 2021, Virtual Event, Austria, May 3-7, 2021*. OpenReview.net, 2021. URL https://openreview.net/forum?id=kvhzKz-_DMF.
- McCoy, T., Pavlick, E., and Linzen, T. Right for the wrong reasons: Diagnosing syntactic heuristics in natural language inference. In *Proceedings of the 57th Annual Meeting of the Association for Computational Linguistics*, pp. 3428–3448, Florence, Italy, July 2019. Association for Computational Linguistics. doi: 10.18653/v1/P19-1334. URL <https://aclanthology.org/P19-1334>.
- Naik, A., Ravichander, A., Sadeh, N. M., Rosé, C. P., and Neubig, G. Stress test evaluation for natural language inference. In Bender, E. M., Derczynski, L., and Isabelle, P. (eds.), *Proceedings of the 27th International Conference on Computational Linguistics, COLING 2018, Santa Fe, New Mexico, USA, August 20-26, 2018*, pp. 2340–2353. Association for Computational Linguistics, 2018. URL <https://aclanthology.org/C18-1198/>.
- Orgad, H., Goldfarb-Tarrant, S., and Belinkov, Y. How gender debiasing affects internal model representations, and why it matters. *CoRR*, abs/2204.06827, 2022. doi: 10.48550/arXiv.2204.06827. URL <https://doi.org/10.48550/arXiv.2204.06827>.
- Ravichander, A., Dalmia, S., Ryskina, M., Metze, F., Hovy, E., and Black, A. W. NoiseQA: Challenge set evaluation for user-centric question answering. In *Proceedings of the 16th Conference of the European Chapter of the Association for Computational Linguistics: Main Volume*, pp. 2976–2992, Online, April 2021. Association for Computational Linguistics. doi: 10.18653/v1/2021.eacl-main.259. URL <https://aclanthology.org/2021.eacl-main.259>.

- Rosenfeld, J. S., Rosenfeld, A., Belinkov, Y., and Shavit, N. A constructive prediction of the generalization error across scales. In *8th International Conference on Learning Representations, ICLR 2020, Addis Ababa, Ethiopia, April 26-30, 2020*. OpenReview.net, 2020. URL <https://openreview.net/forum?id=ryenvpEKDr>.
- Russakovsky, O., Deng, J., Su, H., Krause, J., Satheesh, S., Ma, S., Huang, Z., Karpathy, A., Khosla, A., Bernstein, M., Berg, A. C., and Fei-Fei, L. ImageNet Large Scale Visual Recognition Challenge. *International Journal of Computer Vision (IJCV)*, 115(3):211–252, 2015. doi: 10.1007/s11263-015-0816-y.
- Sanh, V., Debut, L., Chaumond, J., and Wolf, T. Distilbert, a distilled version of BERT: smaller, faster, cheaper and lighter. *CoRR*, abs/1910.01108, 2019. URL <http://arxiv.org/abs/1910.01108>.
- Saphra, N. and Lopez, A. Understanding learning dynamics of language models with SVCCA. In *Proceedings of the 2019 Conference of the North American Chapter of the Association for Computational Linguistics: Human Language Technologies, Volume 1 (Long and Short Papers)*, pp. 3257–3267, Minneapolis, Minnesota, June 2019. Association for Computational Linguistics. doi: 10.18653/v1/N19-1329. URL <https://aclanthology.org/N19-1329>.
- Saxe, A. M., Bansal, Y., Dapello, J., Advani, M., Kolchinsky, A., Tracey, B. D., and Cox, D. D. On the information bottleneck theory of deep learning. In *6th International Conference on Learning Representations, ICLR 2018, Vancouver, BC, Canada, April 30 - May 3, 2018, Conference Track Proceedings*. OpenReview.net, 2018. URL https://openreview.net/forum?id=ry_WPG-A-.
- Schölkopf, B., Janzing, D., Peters, J., Sgouritsa, E., Zhang, K., and Mooij, J. M. On causal and anticausal learning. In *Proceedings of the 29th International Conference on Machine Learning, ICML 2012, Edinburgh, Scotland, UK, June 26 - July 1, 2012*. icml.cc / Omnipress, 2012. URL <http://icml.cc/2012/papers/625.pdf>.
- Shen, Z., Liu, J., He, Y., Zhang, X., Xu, R., Yu, H., and Cui, P. Towards out-of-distribution generalization: A survey. *CoRR*, abs/2108.13624, 2021. URL <https://arxiv.org/abs/2108.13624>.
- Shwartz-Ziv, R. and Tishby, N. Opening the black box of deep neural networks via information. *CoRR*, abs/1703.00810, 2017. URL <http://arxiv.org/abs/1703.00810>.
- Swayamdipta, S., Schwartz, R., Lourie, N., Wang, Y., Hajishirzi, H., Smith, N. A., and Choi, Y. Dataset cartography: Mapping and diagnosing datasets with training dynamics. In Webber, B., Cohn, T., He, Y., and Liu, Y. (eds.), *Proceedings of the 2020 Conference on Empirical Methods in Natural Language Processing, EMNLP 2020, Online, November 16-20, 2020*, pp. 9275–9293. Association for Computational Linguistics, 2020. doi: 10.18653/v1/2020.emnlp-main.746. URL <https://doi.org/10.18653/v1/2020.emnlp-main.746>.
- Tänzer, M., Ruder, S., and Rei, M. BERT memorisation and pitfalls in low-resource scenarios. *CoRR*, abs/2105.00828, 2021. URL <https://arxiv.org/abs/2105.00828>.
- Tishby, N. and Zaslavsky, N. Deep learning and the information bottleneck principle. In *2015 IEEE Information Theory Workshop, ITW 2015, Jerusalem, Israel, April 26 - May 1, 2015*, pp. 1–5. IEEE, 2015. doi: 10.1109/ITW.2015.7133169. URL <https://doi.org/10.1109/ITW.2015.7133169>.
- Tishby, N., Pereira, F. C., and Bialek, W. The information bottleneck method. In *Proc. of the 37-th Annual Allerton Conference on Communication, Control and Computing*, pp. 368–377, 1999. URL <https://arxiv.org/abs/physics/0004057>.
- Tu, L., Lalwani, G., Gella, S., and He, H. An Empirical Study on Robustness to Spurious Correlations using Pre-trained Language Models. *Transactions of the Association for Computational Linguistics*, 8:621–633, 10 2020. ISSN 2307-387X. doi: 10.1162/tacl_a_00335. URL https://doi.org/10.1162/tacl_a_00335.
- Voita, E. and Titov, I. Information-theoretic probing with minimum description length. In Webber, B., Cohn, T., He, Y., and Liu, Y. (eds.), *Proceedings of the 2020 Conference on Empirical Methods in Natural Language Processing, EMNLP 2020, Online, November 16-20, 2020*, pp. 183–196.

- Association for Computational Linguistics, 2020. doi: 10.18653/v1/2020.emnlp-main.14. URL <https://doi.org/10.18653/v1/2020.emnlp-main.14>.
- Wang, B., Wang, S., Cheng, Y., Gan, Z., Jia, R., Li, B., and Liu, J. Infobert: Improving robustness of language models from an information theoretic perspective. In *9th International Conference on Learning Representations, ICLR 2021, Virtual Event, Austria, May 3-7, 2021*. OpenReview.net, 2021a. URL <https://openreview.net/forum?id=hpH98mK5Puk>.
- Wang, J., Lan, C., Liu, C., Ouyang, Y., and Qin, T. Generalizing to unseen domains: A survey on domain generalization. In Zhou, Z. (ed.), *Proceedings of the Thirtieth International Joint Conference on Artificial Intelligence, IJCAI 2021, Virtual Event / Montreal, Canada, 19-27 August 2021*, pp. 4627–4635. ijcai.org, 2021b. doi: 10.24963/ijcai.2021/628. URL <https://doi.org/10.24963/ijcai.2021/628>.
- Zhang, C., Bengio, S., Hardt, M., Recht, B., and Vinyals, O. Understanding deep learning requires rethinking generalization. *arXiv:1611.03530 [cs]*, February 2017. URL <http://arxiv.org/abs/1611.03530>. arXiv: 1611.03530.
- Zhang, X., He, Y., Xu, R., Yu, H., Shen, Z., and Cui, P. Nico++: Towards better benchmarking for domain generalization, 2022. URL <https://arxiv.org/abs/2204.08040>.
- Zhao, Z., Dua, D., and Singh, S. Generating natural adversarial examples. In *6th International Conference on Learning Representations, ICLR 2018, Vancouver, BC, Canada, April 30 - May 3, 2018, Conference Track Proceedings*. OpenReview.net, 2018. URL <https://openreview.net/forum?id=H1BLjgZCb>.

A Computing Information Measures

Our goal is to compute the Entropy for a neuron, A_x , and MI between a pair of neurons, A_x and A_y , for some $(x, y) \in \{1, \dots, N\}$, where the neurons are represented as their activations for a given number of samples (S).

A.1 Entropy

Algorithm 2 Computing entropy

```

1: procedure ENTROPY( $A_x$ )
2:    $H(A_x) \leftarrow 0$ 
3:    $\hat{A}_x \leftarrow \text{BIN}(A(x, i))$  ▷ Discretizing activations by binning
4:   for  $i \in \{1, \dots, N_{bins}\}$  do
5:      $p(\hat{a}_{(x,i)}) \leftarrow \{\mathbb{1}\{\hat{a}_{(x,i)} == \hat{a}_{(x,j)}\}\}_{j=1}^S / S$  ▷ Computing probability
6:      $h(a_{(x,i)}) \leftarrow p(\hat{a}_{(x,i)}) \log(1/p(\hat{a}_{(x,i)}))$  ▷ As per Eq. 1
7:      $H(A_x) \leftarrow H(A_x) + h(a_{(x,i)})$ 
8:   end for
9:    $H(A_x) \leftarrow H(A_x) / S$  ▷ As per Eq. 1
10:  return  $H(A_x)$ 
11: end procedure

```

In order to compute entropy, we first discretize the set of neuron activations by binning them in a uniform range of values (Darbellay & Vajda, 1999). Specifically, we divide the range of activations for a neurons into a constant number of bins (usually 100), each of the same size. Then, the probability for each activation is determined by the number of activations that share the same discrete value. Plugging these values in Equation 1, across all activations for a neurons gives us the entropy for that neuron.

A.2 Mutual Information

To compute the MI between these one-dimensional variables, we use the estimator proposed in Kraskov et al. (2004), which provides a tight lower bound to the mutual information, especially in low-dimensional cases (Belghazi et al., 2018).

Kraskov et al. (2004) consider the popular interpretation of mutual information $I(X; Y)$ between two continuous random variables X and Y as “the amount of uncertainty left in Y when X is known”. In terms of Shannon entropy, this is equivalent to $I(X; Y) = H(Y) - H(Y|X) \equiv H(X) + H(Y) - H(X, Y)$. Following this formalization, we require to work with three variables— A_x , A_y , and $A_z = (A_x, A_y)$. To compute the MI, the k -nearest neighbor distances are considered for these variables. Particularly, for some given distance metric, we represent ϵ_i as the distance of a given point $a_{(z,i)} = (a_{(x,i)}, a_{(y,i)})$ to its k^{th} -neighbor. This distance is then considered in the x and y spaces— $e_{(x,i)}$ and $e_{(y,i)}$ depict the number of points that lie at a distance lesser than ϵ_i with respect to $a_{(x,i)}$ and $a_{(y,i)}$, respectively. Then, the mutual information is given as:

$$I(A_x; A_y) = \psi(k) + \psi(S) - \frac{1}{S} \sum_{i=1}^S (\psi(e_{(x,i)}) + \psi(e_{(y,i)})) \quad (3)$$

where, $\psi(\cdot)$ is the digamma function, or the logarithmic derivative of the gamma function $\Gamma(\cdot)$: $\psi(x) = \frac{\Gamma'(x)}{\Gamma(x)} = \ln x - \frac{1}{2x}$.

We use the Chebyshev distance or the L_∞ metric as our distance metric for all distance computations in the X , Y , and Z spaces.

Popular recent estimators take a neural approach for estimating MI and consider an alternate interpretation of MI as the dependence between two random variables, i.e., $I(X; Y) = D_{KL}(P_{(X,Y)} || P_X \otimes P_Y) = D_{KL}(P_{(Y|X)} || P_Y)$. Since $p(y|x)$ is a-priori unknown for most real-world distributions, Cheng et al. (2020) approximate it through a parametric variational distribution $q_\theta(y|x)$. Belghazi et al. (2018) instead consider representations that estimate the KL divergence. They parameterize the

Algorithm 3 Computing mutual information

```
1: procedure MI( $A_x, A_y$ )
2:    $I(A_x; A_y) \leftarrow \psi(k) + \psi(S)$  ▷ As per Eq. 3
3:    $A_z \leftarrow A_x \oplus A_y$ 
4:    $\text{KNN} \leftarrow \text{KNN}(A_z)$  ▷ Initializing k-nearest neighbor distances
5:    $e_x \leftarrow 0, e_y \leftarrow 0$ 
6:   for  $i \in \{1, \dots, S\}$  do
7:      $\epsilon_i \leftarrow \text{KNN}(a_{(z,i)}).r(k)$  ▷ Distance to the  $k^{\text{th}}$  neighbor
8:      $e_{(x,i)} \leftarrow \{\mathbb{1}\{\|x_j - x_i\| < \epsilon_i\}\}_{j=1}^{X-i}$ 
9:      $e_{(y,i)} \leftarrow \{\mathbb{1}\{\|y_j - y_i\| < \epsilon_i\}\}_{j=1}^{X-i}$ 
10:     $e_x \leftarrow e_x + \psi(e_{(x,i)}), e_y \leftarrow e_y + \psi(e_{(y,i)})$ 
11:  end for
12:   $I(A_x; A_y) \leftarrow I(A_x; A_y) - \frac{1}{|X|}(e_x + e_y)$  ▷ As per Eq. 3
13:  return  $I(A_x; A_y)$ 
14: end procedure
```

family of functions that defines the bound of these representations using a neural network. However, these approaches require us to learn a distinct neural network for each pair of random variable across which we wish to compute the MI. Considering the large number of pairwise operations, especially when working at the level of individual neurons, these approaches are not feasible for our analysis.

B Extended Experimental Details

Table 3: Values for network and training hyper-parameters across different experimental settings.

Model	# Layers	# Parameters	# Epochs	LR	Batch size	Pretrained?
MLP (Colored MNIST)	3	0.232M	50	0.001	512	×
MLP (Shuffled MNIST)	3	0.184M	200	0.001	512	×
DistilBERT	6	66M	20	5e-5	64	✓
RoBERTa-base	12	123M	10	5e-5	64	✓
ResNet-18	18	11M	25	1e-5	64	×

Details for network architectures and training regimes are given in Table 3. Further explanations regarding datasets for the various experimental settings are elaborated below.

B.1 Colored MNIST

All images in the training and evaluation sets are colored green or red. $\alpha \in \{0.00, 0.25, 0.50, 0.75, 1.00\}$ corresponds to the fraction of training examples that follow the color-to-label correlation: green \rightarrow label-0 (digits 0–4) and red \rightarrow label-1 (digits 5–9). The size of the set is same as the original MNIST set, that is a training set of 50k examples and an evaluation set of 10k examples. The hyper-parameters for model training were picked from (Arjovsky et al., 2019).

B.2 Sentiment Adjectives

The chosen set of adjectives for sub-sampling examples from IMDb and then induce the adjective-based spurious correlations are: **Positive**: $\{good, great, wonderful, excellent, best\}$, and **Negative**: $\{bad, terrible, awful, poor, negative\}$. To maintain the correlation for each individual adjective, the set does not contains examples that contain adjectives from both of the sets. The size of this sampled set came to be $\sim 6k$, out of which 67% of the example already abide to the heuristic. That is, the true label corresponding to these examples is same as the nature of adjective(s) they contain. Thus, we vary the labels corresponding to the other 33% of the examples with increasing α . Particularly, α takes a value in $\{0.00, 0.25, 0.50, 0.75, 1.00\}$, where 0.00 suggests that 33% of the data does not follow the heuristic, while 1.00 suggests that all examples follow the heuristic. The learning rate

(LR) and batch size was chosen after a hyper-parameter sweep with values $\{5e-3, 3e-4, 5e-5\}$, $\{16, 32, 64\}$ on the generalizing training set ($\alpha = \beta = 0.00$).

B.3 Bias-in-Bios

We perform our analysis over trained models released by [Orgad et al. \(2022\)](#) for randomly picked random seeds of 0, 5, 26, 42, and 63. Bias-in-Bios ([De-Arteaga et al., 2019](#)) contains around 400k biographies, the networks are trained on 65% of this set, while a sub-sampled balancing from the rest of examples are used for evaluation and analysis.

B.4 NICO++

We sub-sample 6 animal classes with the most number of examples across them (*bear, dog, cat, bird, horse, sheep*) from the original dataset, spanning $\sim 10k$ training and $\sim 7.8k$ evaluation examples. Both balanced and unbalanced set contain all individual contexts for the animals. For the unbalanced set: one from ten common contexts is associated to each of the chosen animal classes (*grass, water, autumn, dim, outdoor, rock*, respectively). On the other hand, the balanced set contains equal number of images from all these contexts for each of the animal classes.

B.5 Shuffled MNIST

Labels are shuffled for the 10 digits of MNIST over the 50k training examples. $\beta \in \{0.00, 0.25, 0.50, 0.75, 1.00\}$. The evaluation and analysis is performed over 10k balanced testing examples from the original set.

B.6 Shuffled IMDb

The networks are trained for the 25k training examples and shuffled for $\beta \in \{0.00, 0.25, 0.50, 0.75, 1.00\}$. Performance computations and analysis is performed on 5k examples sampled from the evaluation set.

C Extended Experimental Results

C.1 Semi-synthetic Heuristic Memorization

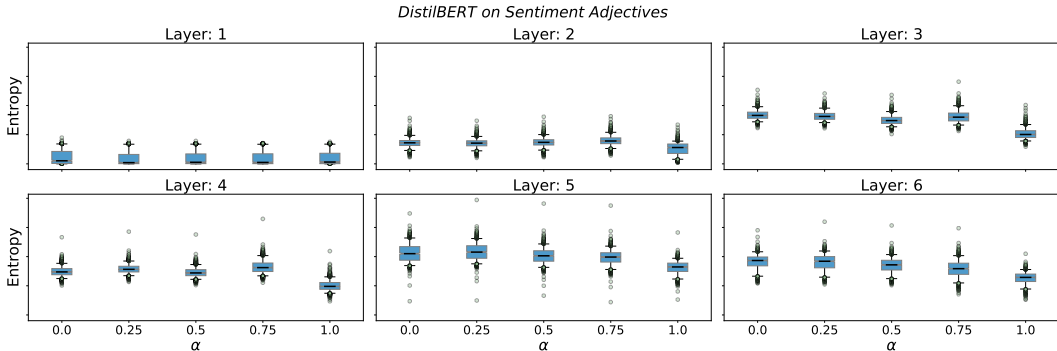


Figure 8: Variation of neuron entropy across all layers of DistilBERT on Sentiment Adjectives.

Figure 8 shows the variation of neuron entropy across increasing values of α (here, adjective-to-sentiment correlation during training) for all layers of DistilBERT. As discussed in the main text (§3.1), we primarily see a variation in entropy for later layers in the network. In the first layer, we observe that entropy for all values of α remains similar and low, while as we go towards the later layers, we start to see certain differences in entropy, with the network for $\alpha = 1.0$ showing especially lower entropy. Since all these networks have been fine-tuned from the same pre-trained initialization and vary only in terms of how much spurious correlation is present in their training sets, we attribute this pattern across layers to a possibility that such spurious correlation are largely captured in the later layers during fine-tuning.

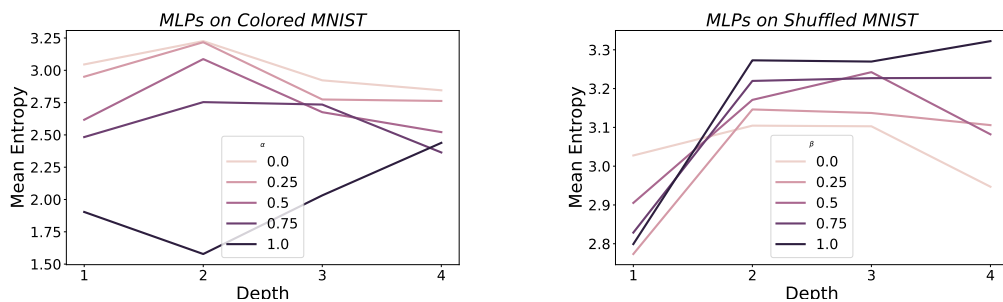


Figure 9: Comparison of entropy for MLP networks with varying number of layers.

C.2 Effect of Model Capacity

Theoretically, we expect that capacity of a network would influence entropy and MI. To test this, we train MLP networks with varying depths for the tasks of Colored MNIST and Shuffled MNIST, and compare the neuron entropy for the obtained networks. From results shown in Figure 9 observe that our hypothesis holds true for all capacities (ranging from single to four-layered networks). However, different capacity networks show entropy values in different ranges and hence they are likely not directly comparable with each other.

C.3 Bias-in-Bios variation across layers

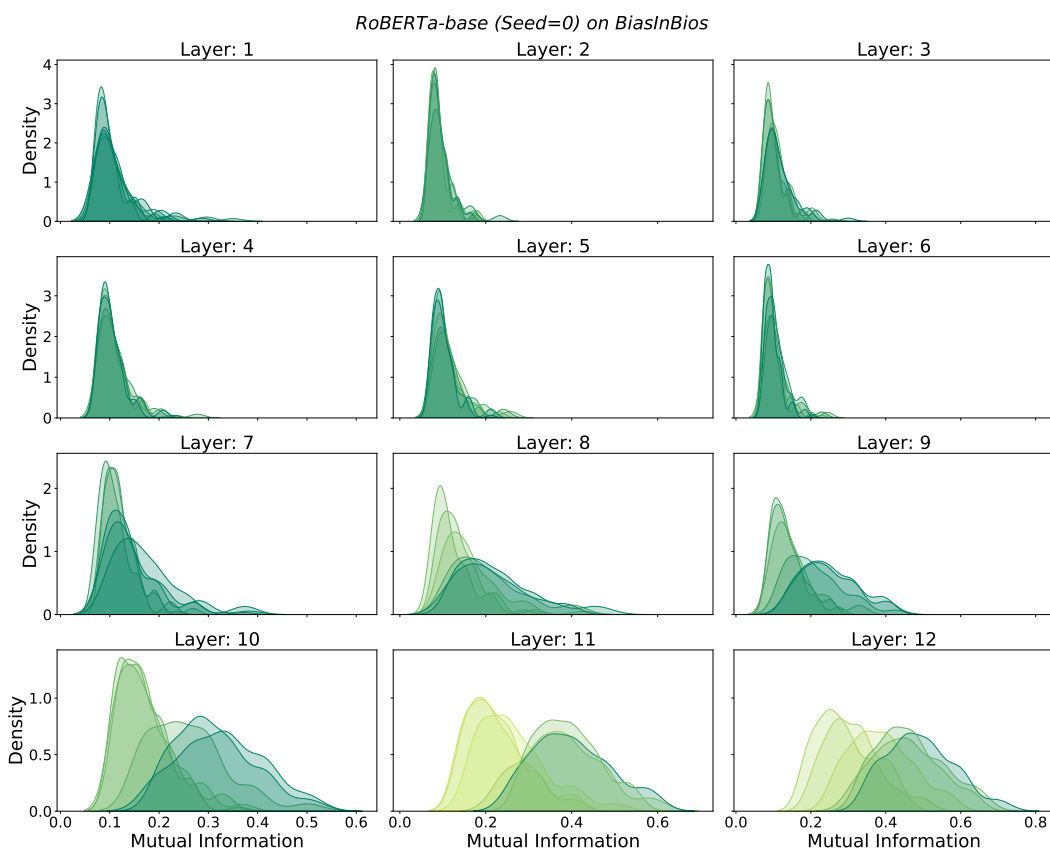


Figure 10: Distribution of MI across neuron pairs for different layers in RoBERTa-base fine-tuned on Bias-in-Bios training sets. Colors represent the value of gender extractability with the MDL probe.

Figure 10 shows how the density of neuron pairs across MI values changes across layers of RoBERTa-base when trained on different training sets of Bias-in-Bios. By looking at these distributions of MI in conjunction with the value of compression (obtained through the MDL probe), we observe a very interesting phenomenon: The relation between MI and compression is maintained throughout the network across its different layers. Networks trained on the different training sets have very similar presence of gender information, as indicated by compression values (color of the Gaussian plots). This is replicated in the MI distribution where all plots are clustered at very similar values. We see that the distinction among the different sets starts to become more lucid with later layers (reflected in the colors) and the same distinction is observed with MI, where more biased models (darker colors) show higher MI. We reported the results for the last layer in the main text (§3.2) because compression values vary the most at this layer, and is consequently reflected in MI. However, looking at the variation across all layers here validates the usage of information measures as a tool for evaluation even strongly.

C.4 Relation to Complexity Measures

Table 4: Pearson correlation coefficient (PCC) between norm-based complexity measures and information measures for the two memorization types.

Complexity Measures	PCC for Colored MNIST		PCC for Shuffled MNIST	
	Mean Entropy	Mean MI	Mean Entropy	Mean MI
2-Norm	0.31	0.14	0.96	1
Frobenius-Norm	0.5	0.31	0.99	0.95
Path-Norm	0.58	0.3	0.98	0.94
Validation Acc.	0.96	0.85	0.87	0.7

Here, we validate that the activation diversity does not simply capture the complexity of a learned model. Popular norm-based measures are often used as complexity measures (also used for model selection; see appendix D.2). On computing the absolute pearson correlation between these complexity measures and our proposed information measures in Table 4, we observe that the two are weakly correlated for Colored MNIST and strongly correlated for Shuffled MNIST. This suggests that the information measures might approximate to model complexity in the case of example-level memorization, but captures more than just complexity as evident for heuristic memorization. Notably, in both cases, our measures are strongly correlated to the validation accuracy.

C.5 Variance of Entropy and MI

As seen from results on our various experimental setups (Figures 1-7), typically a wide distribution of values is observed for both entropy and MI, for all models trained on different α and β values. Since entropy is computed for each neuron in the network and MI for all pairs of neurons, a large number of values are obtained for each network, resulting to this wide distribution. Even though these distributions have a wide range, an observable difference is seen that follows the expected trend across both kinds of memorizations. This is further apparent through the model selection results where even the mean over these two distributions yields encouraging rankings. However, such a variance could make it challenging for practitioners to identify differences in cases when the amount of memorization between two models is not high (for instance, a difference of $\alpha = 0.5$).

D Extended Analysis for Model Selection

D.1 Model Rankings for Bias-in-Bios

Here, we compute the Kendall τ ranking correlations between all ranking metrics for the Bias-in-Bios dataset (Table 5). We observe that extrinsic metrics (TPR, FPR, Separation, and Sufficiency Gap) share higher correlations between each other than those with MI and Entropy, that are only weakly positive. All these extrinsic metrics are computed by training and assessing the networks on specifically curated sets that are labeled for gender information and are thus expected to be more similar to each other. However, we see that compression (an intrinsic metric that still requires labeled data) correlates in a similar manner to extrinsic as well as the information theoretic measures (not requiring labeled data).

Table 5: Kendall’s τ between model rankings from all pairs of intrinsic and extrinsic metrics. τ can range from -1.0 (perfect disagreement) to 1.0 (perfect agreement).

	Comp- ression	TPR Gap	FPR Gap	Separation Gap	Sufficiency Gap	Entropy (Mean)	MI (Mean)
Compression	1.00	0.47	0.60	0.47	0.47	0.47	0.60
TPR Gap	0.47	1.00	0.87	0.73	0.73	0.20	0.07
FPR Gap	0.60	0.87	1.00	0.60	0.60	0.07	0.20
Separation Gap	0.47	0.73	0.60	1.00	1.00	0.20	0.33
Sufficiency Gap	0.47	0.73	0.60	1.00	1.00	0.20	0.33
Entropy (Mean)	0.47	0.20	0.07	0.20	0.20	1.00	0.60
MI (Mean)	0.60	0.07	0.20	0.33	0.33	0.60	1.00

D.2 Comparison with Baseline Generalization Measures

We perform model selection on several benchmark generalization measures. Norm-based measures are popularly used in literature as a measure of generalization (Jiang et al., 2019), and we conduct comparisons with three of them: 2-norm, Frobenius-norm, and Path-norm. We do this for all our setups across example-level and heuristic memorization (Path-norm is not computed on the transformer models, since no established way exists to do so). On comparing the model selection performance with our information measures, we observe that while these baselines (specifically Frobenius-norm and Path-norm) do reasonably well in ranking models that perform example-level memorization, they do poorly for heuristic memorization. This follows from the fact that these metrics are conventionally based and tested on the more widely known notion of memorization, that of individual examples. Where 2-norm gives $\tau = 1$ on Shuffled-IMDb, it is totally uncorrelated ($\tau = 0.00$) for Sentiment Adjectives.

At the same time, our information measures hold positive τ values across all models and tasks, while the baseline measures are inconsistent, varying from extremely low to high values across setups. Frobenius-norm shows perfect negative and positive correlations with Shuffled IMDb and MNIST, respectively, depicting that a high norm value could mean anything depending on the dataset and model.

Table 6: Expanded results for model selection with added Kendall τ ranking correlations for norm-based generalization measures (Jiang et al., 2019).

	Sentiment Adjectives	Colored MNIST	Bias-in-Bios			Shuffled IMDb	Shuffled MNIST
	Validation Accuracy	Validation Accuracy	Comp- ression	TPR Gap	Suff. Gap	Validation Accuracy	Validation Accuracy
Mean Entropy	0.80	1.00	0.47	0.20	0.20	0.60	1.00
Mean MI	0.80	1.00	0.60	0.07	0.33	0.80	1.00
2-Norm	0.00	-0.20	0.33	0.60	0.87	1.00	0.80
Frobenius-Norm	-0.40	0.80	-0.20	0.07	0.07	-1.00	1.00
Path-Norm		0.80					1.00

E Compute Resources and Details

For our experiments that work with MLP networks, we use a single NVIDIA GeForce RTX 2080 GPU (16 GB) to perform the training and inference. For other experiments with larger transformer and convolutional networks—DistilBERT, RoBERTa, and ResNet-18—we use a single NVIDIA A40 GPU (48 GB) to perform fine-tuning/training and inference. We use pre-trained checkpoints from prior work whenever possible and limit the amount of training we do ourselves. In all, we use ~ 190 GPU hours for our experiments, a breakdown of which is given in Table 7.

Table 7: GPU hours used per experiment.

	# Types (Dataset/Training Configurations)	# Seeds/ Type	Training		Inference		Total Time (Hours)
			Time/Run (Hours)	Total (Hours)	Time/Run (Hours)	Total (Hours)	
MLP (Colored MNIST)	5	10	0.25	12.5	0.05	2.5	15
MLP (Shuffled MNIST)	5	10	1	50	0.05	2.5	52.5
DistilBERT (Sentiment Adjectives)	5	5	1	25	0.20	5	30
DistilBERT (Shuffled IMDB)	5	5	2.5	62.5	0.20	5	67.5
RoBERTa-base	5	5	-	-	0.5	12.5	12.5
ResNet-18	2	5	1	10	0.25	2.5	12.5
Total GPU Time							190

F Potential Societal Impacts

Our work is aimed at comparing a given set of models by shedding light on their potential reliance on two facets of memorization. While such evaluation is meant to be used to pick the best model, (for instance, the least biased one) one could instead use it to choose the least generalizing model (the most biased). This can be especially worrisome in sensitive scenarios like that of gender bias, where one could easily switch the order of entropy and MI to obtain a network which attends to gender information the most.

G Dataset Licenses

All datasets used in this work are freely publicly available.

Bias-in-Bios: MIT License

MNIST: GNU General Public License v3.0

IMDb: License statement can be found [here](#).

NICO: License statement can be found [here](#).